water

MDPI

Article

Radon and Salinity Mass Balance Constraints on Groundwater Recharge on a Semi-Arid Island (Catalina, California)

Benjamin Hagedorn * and Mitsuyo Tsuda

Department of Geological Sciences, California State University, Long Beach, CA 90840, USA; mitsuyo.tsuda@student.csulb.edu

* Correspondence: klaus.hagedorn@csulb.edu; Tel.: +1-562-985-4198

Abstract: Quantifying the freshwater component of submarine groundwater discharge (SGD) is critical in the analysis of terrestrial influences on marine ecosystems and in assessing the water budget and groundwater recharge of coastal aquifers. In semi-arid to arid settings, this quantification is difficult because low SGD rates translate into low concentrations of groundwater solutes in coastal waters. In this study, fresh SGD (FSGD) was quantified for Toyon Bay on Catalina Island, California, for wet and dry seasons using a combination of radon and salinity mass balance models, and the results were compared to watershed-specific groundwater recharge rates obtained from soil water balance (SWB) modeling. Calculated FSGD rates vary only slightly with season and are remarkably similar to the recharge estimates from the SWB model. While sensitivity analyses revealed FSGD estimates to be significantly influenced by uncertainties in geochemical variability of the groundwater end-member and fluctuations of water depth, the results of this study support the SWB-model-based recharge rates. The findings of this study highlight the utility of the radon-and-salinity-mass-balance-based FSGD estimates as groundwater recharge calibration targets, which may aid in establishing more refined sustainable groundwater yields.

Keywords: water balance; submarine groundwater discharge; drylands; sustainable groundwater yield; drought

Citation: Hagedorn, B.; Tsuda, M. Radon and Salinity Mass Balance Constraints on Groundwater Recharge on a Semi-Arid Island (Catalina, California). *Water* **2022**, *14*, 1068. https://doi.org/10.3390/w14071068

Academic Editor: Juan José Durán

Received: 11 February 2022
Accepted: 22 March 2022
Published: 28 March 2022

1. Introduction

Submarine groundwater discharge (SGD) can be an important contributor of solutes to coastal marine ecosystems, especially in semi-arid to arid settings with low river discharge [1–3]. One of the SGD components is fresh meteoric water that infiltrates the subsurface, recharges the coastal aquifer, and discharges along the coast through the hydraulic gradient. The other major component of SGD is seawater that infiltrates the seabed and eventually returns to the ocean through a combination of wave set-up, tidal pumping, and convection.

Because of the complexity associated with the quantification of different SGD components, recent research has focused on capturing the spatiotemporal SGD variability at small (i.e., coastal inlet) scales. Spatial variation in SGD has been linked to pumping-related perturbation of the groundwater flow system [4], varying rates of groundwater recharge [5], and aquifer heterogeneity, or the distribution of high- and low-permeability coastal aquifers [6,7]. Several studies ([1], and references therein) explicitly highlight the complexity associated with conduits and fractures on SGD mechanisms and locations in karstic coastal aquifers.

Temporal variation in SGD is related to the changes in the hydraulic gradient. An increase in net precipitation leads to higher recharge, which moves the water table upward and the freshwater-seawater interface seaward [8]. As a result, SGD rates tend to be higher during the rainy season, but are sometimes out of phase with precipitation due to the time lag caused by the infiltrating water moving through the unsaturated zone and from

the recharge location to the coast [9]. On shorter time scales, a decrease in sea-surface height from tidal cycles results in a steeper hydraulic gradient, thus enhancing the fresh groundwater flow towards the ocean. For example, in the northern Gaza Strip of Palestine, SGD rates varied from 0 to 6 cm/day within a tidal cycle [4].

The quantification of fresh SGD (FSGD), particularly in temperate-humid and tropical settings, has received increased attention because of the ability of FSGD to transport nutrients and pollutants from the land to the ocean [10–12] and the associated impacts on coastal ecosystems [13,14]. However, in arid to semi-arid settings, this quantification is complicated because of the low inflow and associated difficulties in the detection of freshwater-derived solutes. Recirculated seawater discharge (RSGD) dominates these settings [2,15] and has been shown to also play a significant role in the delivery of nutrients from the shoreline to the ocean [16,17]. More studies on the mechanisms and rates of FSGD in these settings are needed, not only for refined assessments of solute discharge and sources, but also for improved appraisals of freshwater availability. This is important as many coastal regions in more arid climates have become increasingly threatened by groundwater overdraft and seawater intrusion [18–20].

Multiple methods have been applied in quantifying FSGD on various scales. Seepage meters have been used for direct measurement of SGD, but a clear identification of discharge points (i.e., seeps) can be difficult, particularly as it relates to capturing the wide spatial and temporal variability of SGD at the watershed scale [21]. The use of Darcy's Law and numerical modeling requires a reasonable estimate of the aquifer hydraulic conductivity, which is challenging due to heterogeneity in local geology [7]. While the use of radon-222 (hereafter referred to as "radon") mass balance has become popular for SGD research, this method is not sufficient in determining the relative contributions of FSGD from the terrestrial aquifer and RSGD from tidal pumping and is therefore used in combination with another method such as salinity mass balance [22,23]. Other limitations of the conventional radon mass balance method include the difficulty of constraining tidal influence on radon and salinity inventories and uncertainty in the terrestrial groundwater radon signature [23,24].

The objective of this study is to quantify FSGD along a coastal watershed on Santa Catalina Island, California (hereafter referred to as "Catalina"), to refine recent estimates of groundwater recharge. Characterized by low annual precipitation and visited by more than a million tourists each year, the island has been severely affected by water rationing measures to alleviate the water scarcity impact from a recent drought. Two surface water reservoirs, 10 groundwater wells, 13 storage tanks, and two desalination plants provide potable water. Despite concerns regarding a continuing drought and rising demand for usable water, only a few hydrological studies have been conducted on the island to date. Two studies established a radon mass balance-based box model [25,26] to describe water exchange in Catalina Harbor, where benthic input (i.e., molecular diffusion from the sediments enhanced by bioirrigation) and tidal pumping were identified as primary sources of radon, and FSGD was considered negligible. In the study by Harlow and Hagedorn [27], a soil water balance (SWB) model was applied to simulate and map the spatial distribution of groundwater recharge at the island scale during severe drought years. While their study estimated low recharge rates ranging from 0.05 to 82.3 mm/year for the model years 2008 to 2014, the lack of independently constrained calibration data for recharge resulted in significant uncertainty in the recharge predictions.

This study focuses on Toyon Bay, a 3-km^2 watershed on the eastern coast of Catalina that is characterized by above-average annual rainfall and groundwater recharge and pristine, largely undisturbed land cover. FSGD was quantified for wet (spring 2019) and dry (fall 2019) seasons using a non-steady-state mass balance model that combines radon, salinity, and water depth time-series data from two stationary sites with spatial survey data. Special attention was paid to account for the effects of the variability in nearshore groundwater chemistry and water depth on the FSGD quantification. The FSGD rates computed herein were compared to the results from similar settings and to the watershed-

specific recharge estimates from the SWB model to explore the viability of the method for obtaining FSGD and coastal groundwater recharge estimates in comparable settings.

2. Materials and Methods

2.1. Study Area

Catalina is located in the Pacific Ocean about 75 km southwest of Los Angeles, California. The Catalina Island Conservancy owns 88% of the island to maintain its undeveloped nature [28]. The island is an exposed crest of one of the northwest-trending ridges bounded by the strike-slip faults in the California Continental Borderland [29]. Characterized by rugged topography, a large ridge running from the northwest to the southeast serves as an asymmetric drainage divide, with shorter and steeper stream valleys on the eastern side and longer streams on the western side.

The island comprises three dominant rock types: Catalina Schist, Catalina Pluton, and mafic to intermediate volcanic rocks (Figure 1). Most of the northwestern part of the island is occupied by the Catalina Schist, a Mesozoic basement complex consisting of blueschist, greenschist, and amphibolite [30]. On the southeastern part of the island is an exposure of the Catalina Pluton, a quartz diorite intrusion of Miocene age. Various volcanic rocks of Miocene age, mainly of andesitic and dacitic composition, cover the central part of the island and are the remnants of a small volcanic archipelago. Deposits of Tertiary marine and non-marine sedimentary rocks and Quaternary landslides and alluvium are scattered towards the coastal lowlands [29].

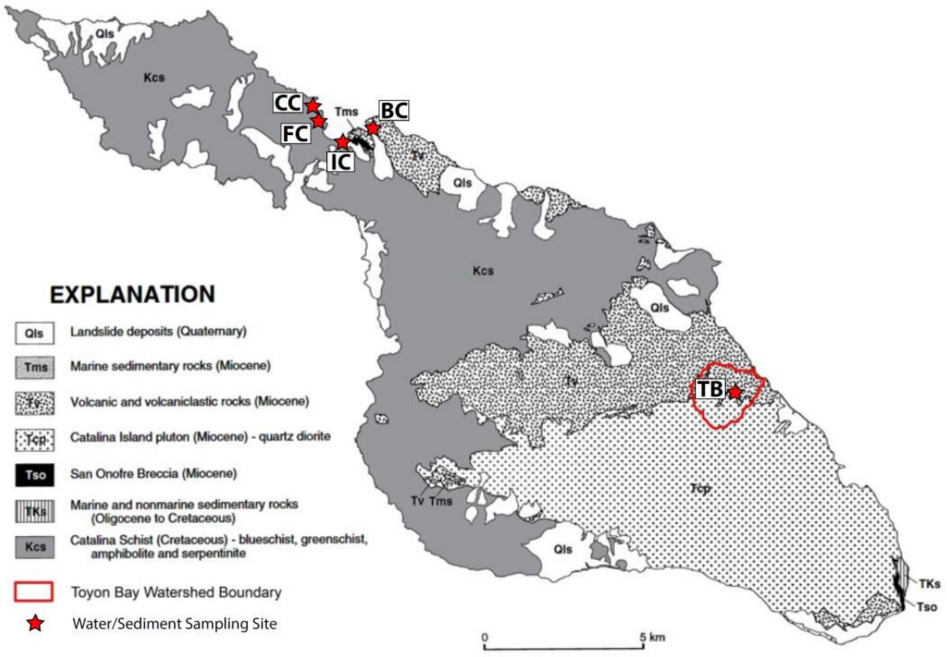

Figure 1. Generalized geologic map of Catalina Island (modified from [29]). Locations of groundwater sample collected at Toyon Bay (TB) and beach sand samples for radon incubation analyses collected at Cherry Cove (CC), Fourth of July Cove (FC), Isthmus Cove (IC), and Big Fisherman's Cove (BC) are highlighted.

The climate is semi-arid Mediterranean with warm, dry summers and mild, wet winters. Mean monthly temperatures for the years 1948 to 2016 at Avalon Airport ranged from 11.9 °C in January to 21.7 °C in August [27]. Strong northwesterly winds and coastal eddies reflect the combination of steep topography, high atmospheric pressure gradients, and coastal profile. A thick, low fog bank often envelopes the southern and western coast, causing a sharp altitude contrast in vegetation and soil type. Streams are almost all non-perennial and flow only during and shortly after intense rain events in the winter

months (November through March). Spatial patterns of groundwater recharge, with higher values towards the upper eastern flanks of the main divide, reflect orographic effects and land cover patterns, with herbaceous grassland and "developed, open space" particularly favoring recharge [27].

Toyon Bay is located on the eastern coast in an area covered predominantly by volcanic lithologies. The bay is surrounded by steep mountain fronts providing shelter from the wind, resulting in calm waters year-round. The beach is mostly sandy, with a small rocky area on the northern side near the outlet of a non-perennial stream (Figure 2). Mean annual precipitation in the watershed for the years 1981 to 2010 was 35 cm, slightly higher than the island-wide mean annual precipitation of 33 cm [31]. According to PRISM precipitation [31] and MODIS evapotranspiration data [32,33], evapotranspiration exceeds precipitation in Toyon Bay from March to November. Mean annual groundwater recharge in the watershed, based on the SWB model for the years 2008 to 2014, was 22.6 mm/year, with highest values in the northern parts of the watershed [27].

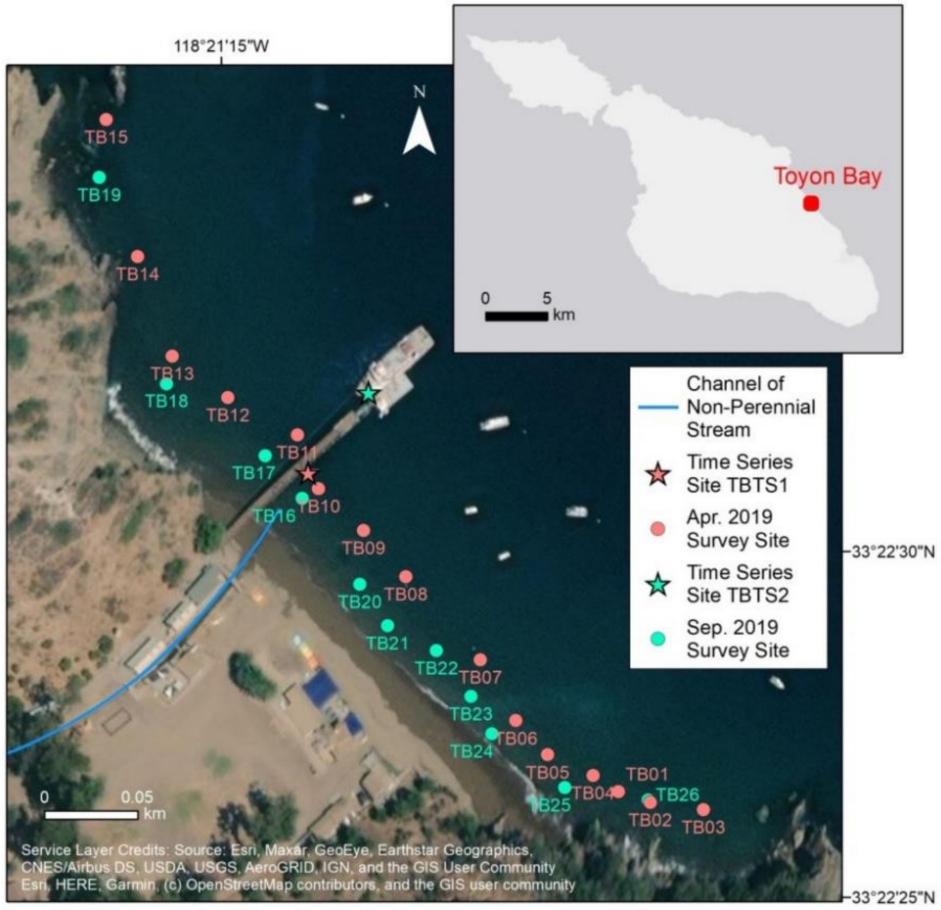

Figure 2. Radon time-series and spatial survey sites in Toyon Bay, California.

2.2. Methods

This study focuses on the use of radon, a volatile decay product of radium-226, as a tracer for quantifying SGD and groundwater recharge assuming no influence of pumping on the hydraulic gradient. While radon in surface water rapidly escapes to the atmosphere, radioactive radon decay in groundwater is balanced by the decay of radium-226 and release of radon from the subsurface mineral grains to the pore space [34,35], resulting in elevated radon levels in SGD-impacted seawater.

2.2.1. Radon Analysis

The RAD-7/RAD AQUA radon system, developed by Durridge Co., Inc. (Billerica, MA, USA), was used to continuously measure activities of polonium-218 and polonium-214 as an indication of dissolved radon activities. The system was connected to a Rule 1100 GPH bilge pump to continuously measure radon activities in the water stream. For the spatial surveys, the system was moved in a kayak in shallow water along the shoreline. The kayak was stopped at each survey site for a measurement over several 15-min counting cycles (Figure 2).

Before beginning the radon measurement at each site, the RAD-7 was purged to clear the chamber of the radon and any decay products from the previous measurement. Then, the first measurement cycle was ignored to accommodate the response delay of the RAD-7 due to the time required to achieve radon concentration equilibrium between water and air at the closed air loop and the time required to achieve radioactive equilibrium between radon and polonium-218 in the chamber [36]. For the spatial surveys, two or three measurement cycles were used at each site to compute radon activities (Tables S1 and S2). For the time-series dataset, continuous measurements were collected at Toyon Pier (Figure 2) in May and September 2019 for 24 and 16 h, respectively (Tables S3 and S4). Water temperature and salinity data were obtained using an InSitu AquaTroll 600 multi-parameter probe.

To discern the applicable groundwater radon end-member concentration for the SGD flux calculation, three datasets were considered: (1) previously reported saline groundwater radon data from beach piezometers installed within and below the tidal zone of Catalina Harbor (located ~15 km northwest of Toyon Bay) [26], (2) radon activities of groundwater sampled in this study at Toyon Spring (located ~870 m west of the Toyon Bay shoreline), and (3) radon activities obtained from incubation experiments of beach sand samples collected at Cherry Cove (CC), Fourth of July Cove (FC), Isthmus Cove (IC), and Big Fisherman's Cove (BC) in July 2018 (see Figure 1 for sample locations). For the incubation experiments, we followed the methods outlined previously [37] and mixed each sample sediment with seawater to create a slurry, which was stored in a sealed bottle for 30 days to allow dissolved radon to reach equilibrium with the radium-226 in the sediment. The equilibrium radon concentration in pore water was estimated using measured radon emanation rate, sediment porosity, and sediment density [26].

2.2.2. Radon Mass Balance Model

This study combined time-series SGD constraints from a non-steady-state radon mass balance model [22] with spatial snapshot radon inventories to produce mean SGD estimates (F_{SGD} in dpm/m^2/day) for the Toyon Bay shoreline for two (spring and fall 2019) sampling campaigns. Results are shown in Figure 3 and listed in Supplementary File S1. The non-steady-state model computes F_{SGD} as a function of changes in the dissolved radon inventory (I) of the time-series dataset [38]:

$$\frac{dI}{dt} = F_{SGD} + F_{tide} + F_{sed} - F_{atm} - F_{dec} - F_{mix} \quad (1)$$

where dI/dt (dpm/m^2/day) is the difference in the inventory between two successive measurements (~1 h) and F_{tide}, F_{sed}, F_{atm}, F_{dec} and F_{mix} correspond to the radon fluxes (dpm/m^2/day) of tidal current input and output, diffusion from seafloor sediments, atmospheric degassing (evasion), radioactive decay, and lateral mixing with radon-depleted offshore waters, respectively. F_{dec} was considered negligible over the short measurement period of this study.

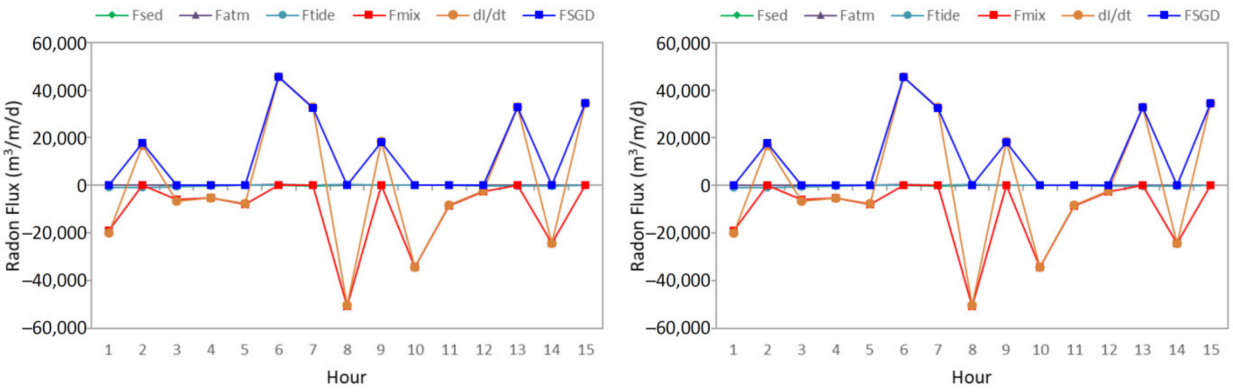

Figure 3. Net radon flux (calculated as $dI/dt - F_{tide} - F_{sed} + F_{atm}$) and mixing loss: (**a**) spring 2019 time-series at site TBTS1; (**b**) fall 2019 time-series at site TBTS2. Note that mixing is considered a loss only when the net radon flux < 0.

The radon inventory, *I*, was calculated by multiplying the measured radon activity in water (C_w), corrected for radon inputs from offshore radium-226 (C_o = ~99.6 dpm/m^3, [25,26]), by the water depth. This approach assumes a non-stratified (i.e., well-mixed) water column. F_{tide}, the inflow and outflow of radon during flood and ebb tides, respectively, was calculated following [39] by multiplying changes in water depth by the radon activity offshore during high tide and radon activity in nearshore waters during low tide. F_{sed} corresponds to the diffusive radon flux that occurs when a radon activity gradient between pore water in the seabed sediment and overlying ocean water exists ($C_{sed} > C_w$) and was calculated following [6,40] by using the radon decay constant (0.181 day^{-1}), the sediment porosity (n = 0.40 for Catalina Harbor beach sand samples [25,26]), the molecular diffusion coefficient of radon in water (estimated empirically using measured water temperature data [41]), and C_{sed} and C_w, with C_{sed} set to the radon activity in the terrestrial groundwater end-member (see Section 2.2.5). Likewise, F_{atm} was indirectly estimated [42] based on gas transfer velocity (calculated using data on wind speed obtained for Avalon from NOAA's National Centers for Environmental Information website and the temperature-dependent Schmidt number [43]), radon concentrations in water and air, and the Ostwald solubility coefficient [22]. After accounting for F_{tide}, $F_{sed,}$ and F_{atm}, F_{mix} was calculated as the maximum negative radon fluxes over time [44], considering it a radon sink only when the net dI/dt (dI/dt that accounts for F_{tide}, $F_{sed,}$ and F_{atm}) was negative (Figure 3). Importantly, this approach provides a lower limit of F_{SGD} because mixing could not be reasonably quantified when the net dI/dt was positive.

2.2.3. Tidal Correction and Scaling of Spatial Survey Radon Data

To capture the spatial pattern of SGD along a shoreline, results from the non-steady-state radon mass balance model (Equation (1)), which are usually limited to only a few time-series datasets, were spatially extrapolated and upscaled using radon inventories (I). This assumes that any difference between the spatial survey snapshot inventories and the inventories of the time-series data over a tidal cycle is caused only by F_{SGD} and F_{tide}. To account for the effect of the latter, the time-series data compiled during the spring and fall 2019 sampling campaigns were used to tide-normalize the respective spatial survey data. The tidal stage of each survey site or time-series hour was estimated based on its relative position to the low and high tide points on the tide graph (Figure 4) using tide data from NOAA's Tides and Currents website, Station ID: 9410079, Avalon (see "Matched Time-Series Site_Hour" in Appendices A and B).

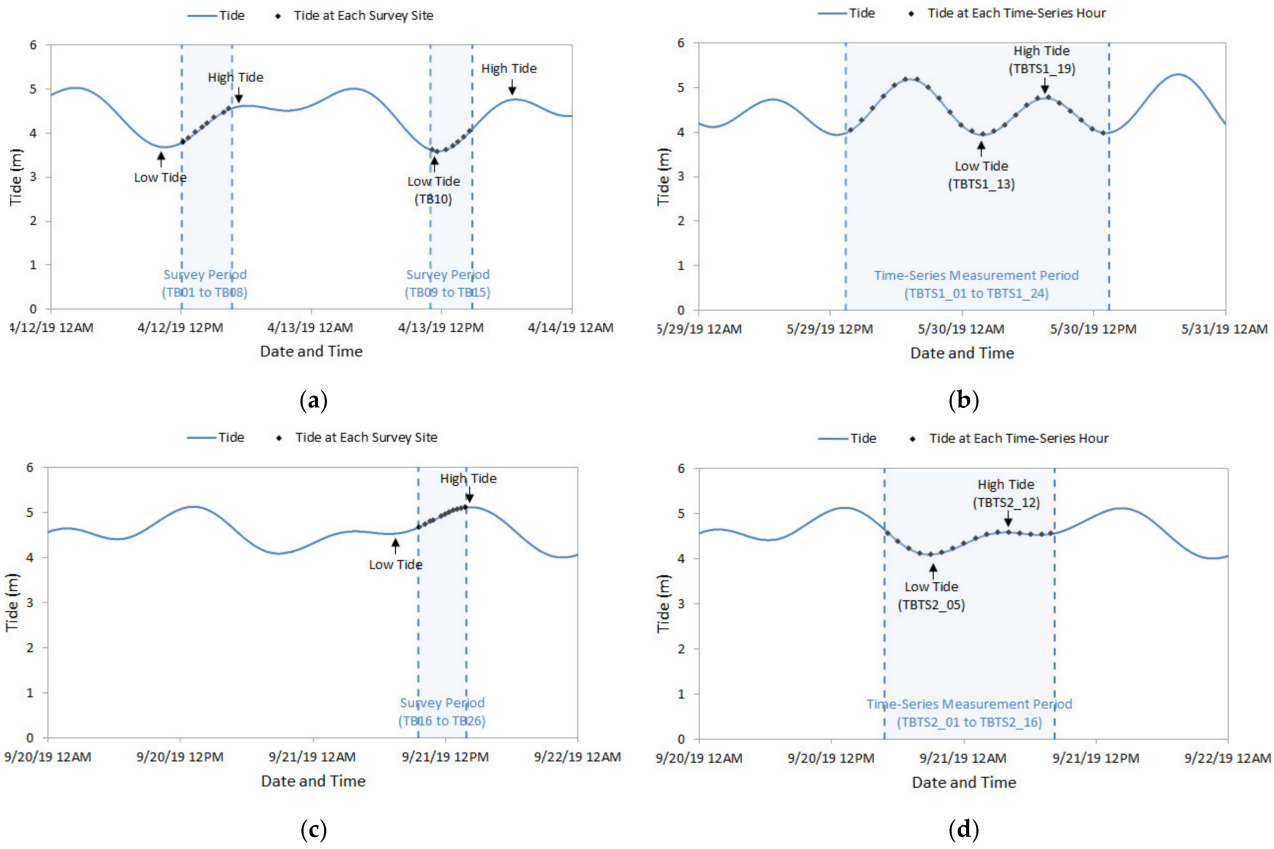

Figure 4. Tide graphs: (**a**) April 2019 spatial survey periods; (**b**) May 2019 time-series measurement period at site TBTS1; (**c**) September 2019 spatial survey period; (**d**) September 2019 time-series measurement period at site TBTS2.

For each survey site, the tide-corrected radon inventory in water, I_{wc} (dpm/m^2), was calculated as

$$I_{wc} = C_w h_w \left(\frac{I_{tsh}}{I_{mean}} \right) \quad (2)$$

where C_w (dpm/m^3) and h_w (~0.7 m) are the measured radon activity and the depth of the water, I_{tsh} (dpm/m^2) is the radon inventory for the time-series hour with matching tidal stage, and I_{mean} is the mean radon inventory of the time-series for the tidal period. The ratio of I_{tsh} to I_{mean} takes into account the temporal variation of the radon activities associated with different tidal stages.

Based on the tidal correction, the mean SGD rate across the Toyon Bay shoreline, $F_{SGD\ mean}$ (dpm/m^2/day), was calculated as

$$F_{SGD\ mean} = F_{SGD} \left(\frac{I_{wc\ mean}}{I_{mean}} \right) \quad (3)$$

where F_{SGD} (dpm/m^2/day) is the SGD rate over a tidal cycle and $I_{wc\ mean}$ (dpm/m^2) is the mean tide-corrected spatial survey radon inventory.

2.2.4. SGD Flux Estimation

The SGD water flux, F_{SGDw}, i.e., the daily volumetric discharge per meter of shoreline (m^3/m/day), can be calculated as [22]

$$F_{SGDw} = \frac{F_{SGD}}{C_{GW}} \left(\frac{A}{L} \right) \quad (4)$$

where C_{GW} represents the terrestrial groundwater end-member, A (m^2) is the area of the corresponding coastal box, and L (m) is the length of this box along the shoreline. A coastal box was defined at each survey site by the average water depth around that survey site, the perpendicular distance from the shoreline, and the sum of the half distance from the previous survey site and the half distance from the next survey site along the shoreline.

To quantify the freshwater and seawater portions of the total SGD water flux, a two-end-member mixing analysis was applied as

$$1 = f_s + f_f \quad (5)$$

$$S_m = S_s f_s + S_f f_f \quad (6)$$

where f_s is the RSGD fraction, f_f is the FSGD (i.e., groundwater recharge) fraction, S_m is the salinity of coastal water (a mix of freshwater and seawater), S_s is the salinity of offshore water (seawater), and S_f is the salinity of terrestrial water (freshwater).

2.2.5. Definition of Groundwater Radon End-Member

Estimating the groundwater radon end-member (C_{GW} in Equation (4)) in RSGD-dominated settings represents a key challenge. Ideally, one should perform concurrent groundwater and surface water measurements of radon, which was not possible during this study. Many previous studies from comparable settings applied fresh groundwater radon data from inland wells for C_{GW}. This can be problematic as groundwater, even in apparently monolithologic aquifer regimes, can exhibit vast concentration gradients [45,46] due to various factors including aquifer porosity, texture, and excess air content [47]. More importantly, SGD dominated by tidally recirculated seawater tends to exhibit significantly lower radon concentrations than fresh groundwater [25,46,48], but still significantly higher values than seawater, e.g., [48] due to radon emanation from beach sediments in the tidal wedge and mixing with high radon saline groundwater from the transitional zone at the base of the freshwater lens. These observations also manifested themselves in this study as we encountered a large spread in fresh groundwater radon concentrations measured at Toyon Spring (~110,000 dpm/m^3) and determined from beach sand incubation experiments (49,000–267,000 dpm/m^3; mean: 119,000 dpm/m^3; 1 standard deviation = 100,000 dpm/m^3). These values were generally higher than those measured in saline groundwater sampled between the high and low tide marks off Catalina Harbor (39,000 ± 11,000 dpm/m^3) [26]. Interestingly, [26] estimated a water–beach sand contact time for these groundwater samples of 0.7–2 d (mean: 1.33 d). Additionally, a mass balance assessment on the basis of a coastal radon budget [25] and a tidal pumping water flux estimate [26] for the head of Catalina Harbor also yielded a low radon concentration of water draining out of the tidal wedge of 57,000 ± 20,000 dpm/m^3 [26]. In light of these findings and recommendations of previous studies from similar tidal pumping-dominated settings [46,48], we selected Colbert et al.'s [26] value of 57,000 dpm/m^3 as the most appropriate radon end-member concentration for SGD at Toyon Bay. The effect of lower and higher radon concentrations from our incubation experiments on the SGD flux estimate was tested in a subsequent sensitivity study.

2.2.6. SWB Data Extraction

To compare the FSGD water fluxes calculated in this study to the groundwater recharge rates estimated by the SWB model [27], the SWB raster data were processed to extract the 2008–2014 mean for Toyon Bay (22.6 mm/year), which was then converted to a volumetric flux using surface area (3.02×10^6 m^2) and shoreline length (540 m) of the watershed. The same calculation was performed for the whole island using the island-wide mean recharge (22.2 mm/year), area (1.96×10^8 m^2), and shoreline length (9.22×10^4 m).

3. Results and Discussion

3.1. Radon and Tide Correlation

The May and September 2019 radon times-series ranged from 0.17 to 3.5 dpm/L (mean: 1.3 dpm/L) and from 0.04 to 0.79 dpm/L (mean: 0.28 dpm/L), respectively. Both time-series appeared to follow a cyclic pattern similar to a tidal cycle (i.e., period of approximately 12 h), with the highest values observed near the low tides and the lowest values observed near the high tides (Figure 5). While there was no significant correlation between the measured radon activity in water and the tidal height, there appeared to be a phase lag between the two datasets. In addition to this general cyclic pattern, high-frequency oscillations were observed in the radon data (green signal in Figure 5), which appeared to occur every measurement cycle (15-min cycles for the May 2019 time-series and 20-min cycles for the September 2019 time-series). To what degree these oscillations may reflect the radioactive signal or technical specifics of the equipment (e.g., oscillations in battery voltage and/or variability in pumping rates) is not fully clear, so further research is needed to identify the sources of these high-frequency oscillations.

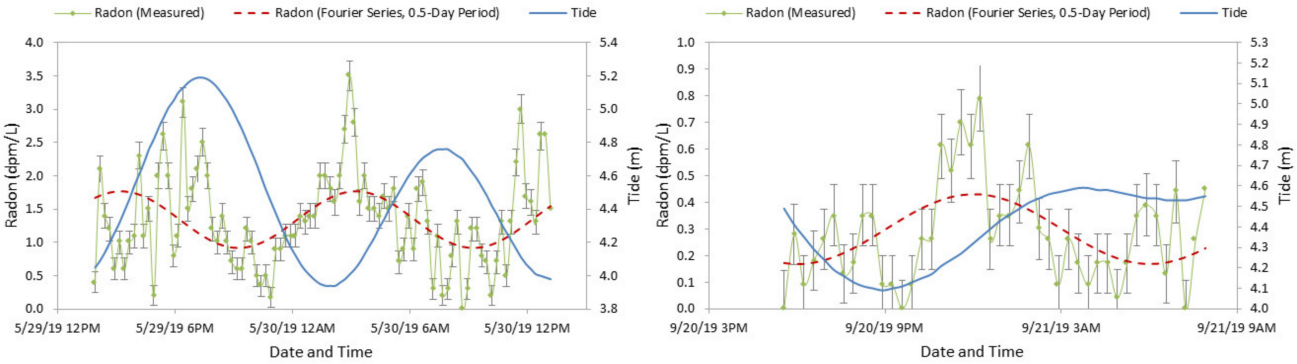

Figure 5. Temporal variation of radon activity in water and tidal height: (**a**) site TBTS1; (**b**) site TBTS2. To view a general shape of the graph, a Fourier series (sum of sine and cosine functions) with half-day period was fit to the radon data using the MATLAB Curve Fitting app.

In a cross-correlation analysis, a significant correlation ($p < 0.05$) was found between the radon activity in water and the tidal height when the May 2019 radon time-series data had lags of −51, −28, −8, 12, or 36 time steps (Figure 6a) and when the September 2019 radon time-series data had a lag of −10 or 10 time steps (Figure 6b). The correlation could be either positive or negative depending on the lag because of the cyclicity in both datasets, but negative correlation was more prevalent. The largest negative correlation was found when the May 2019 radon time-series data had a lag of −8 time steps (i.e., 120 min) and when the September 2019 radon time-series data had a lag of −10 time steps (i.e., 200 min), which indicates that the highest radon activities in water lag the low tides and the lowest radon activities in water lag the high tides, by 2 to 3 h (Figure 7).

The lag of the peak radon activities in water after the low tides may be due to the recirculated seawater moving out through a shallow coastal aquifer in response to tidal pumping [22]. The longer lag time in the September 2019 data could be related to the more attenuated tidal range and the different distances from the shoreline (Figure 2). Inflow of fresh groundwater during the low tides is less likely a major process as it should be accompanied by a significantly shorter lag time and higher radon values [6,10,48]. Similar negative correlation and phase lag between the radon and tide data were observed in other coastal studies, more commonly in the cases where the measured radon values were low or where SGD was strongly driven by tidal pumping [5,49]. Lower radon values tend to have a larger scatter in data because of lower sensitivity of the measurement and larger effects of waves, tides, and currents [10]. As observed in Xiangshan Bay, China, the data from different sites may show different lag times attributed to the varying tidal cycles,

distances from the shoreline, and topographic conditions, causing some sites to have longer SGD transportation distance and smaller SGD-bottom seawater gradients [50]. The phase lag seen in the Toyon Bay data is consistent with the hypothesis that tidal pumping is the primary SGD mechanism in this part of the island.

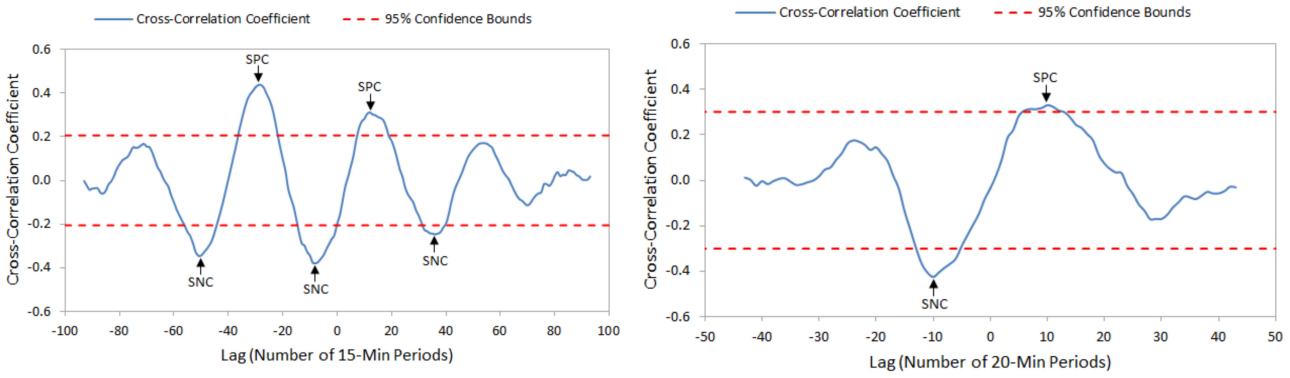

(**a**) (**b**)

Figure 6. Cross-correlation coefficient for each lag of radon activity in water relative to tidal height, with upper and lower bounds of the 95% confidence interval: (**a**) site TBTS1; (**b**) site TBTS2. SPC are the points of significant positive correlation, and SNC are the points of significant negative correlation.

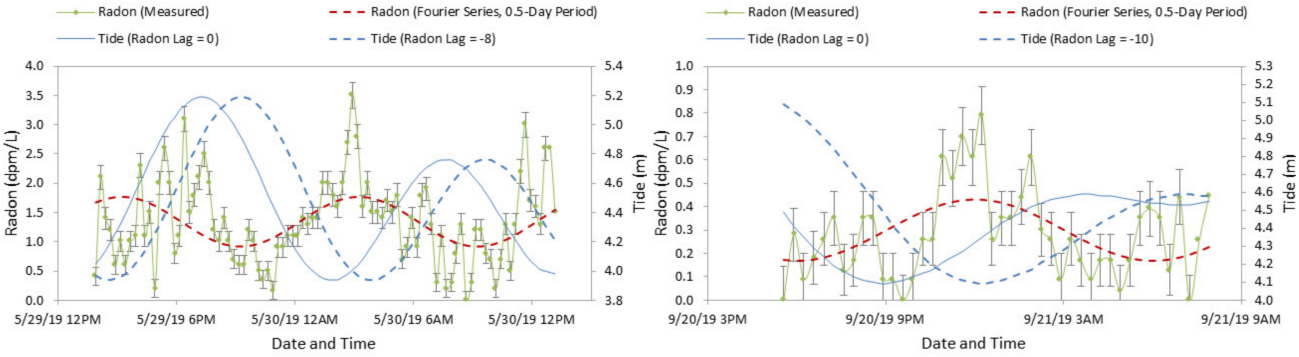

(**a**) (**b**)

Figure 7. Temporal variation of radon activity in water and tidal height, with radon lag: (**a**) site TBTS1, radon lag 0 (original position), and radon lag −8 counting cycle time steps (tide graph shifted to the right by 120 min, or 2.0 h); (**b**) site TBTS2, radon lag 0 (original position), and radon lag −10 time steps (tide graph shifted to the right by 200 min, or 3.3 h).

3.2. Spatial Survey Radon Patterns and Calculated SGD Fluxes

The radon activities in water measured during the April and September 2019 spatial surveys ranged from 0.20 to 8.5 dpm/L (mean: 2.5 dpm/L) and from 0.40 to 3.3 dpm/L (mean: 2.1 dpm/L), respectively, with highest values observed near the non-perennial stream and the gravel-rich northern beach section (Figure 8a). September 2019 activities were lower and more evenly distributed than the values obtained in April 2019. Tide-normalized, the April 2019 values ranged from 0.31 to 9.1 dpm/L (mean: 2.9 dpm/L), and the September 2019 values ranged from 0.53 to 8.1 dpm/L (mean: 3.3 dpm/L) (Figure 8b). The tidal correction increased the mean and range of the radon activities in water, further emphasizing the highest values observed in the northern part of Toyon Bay.

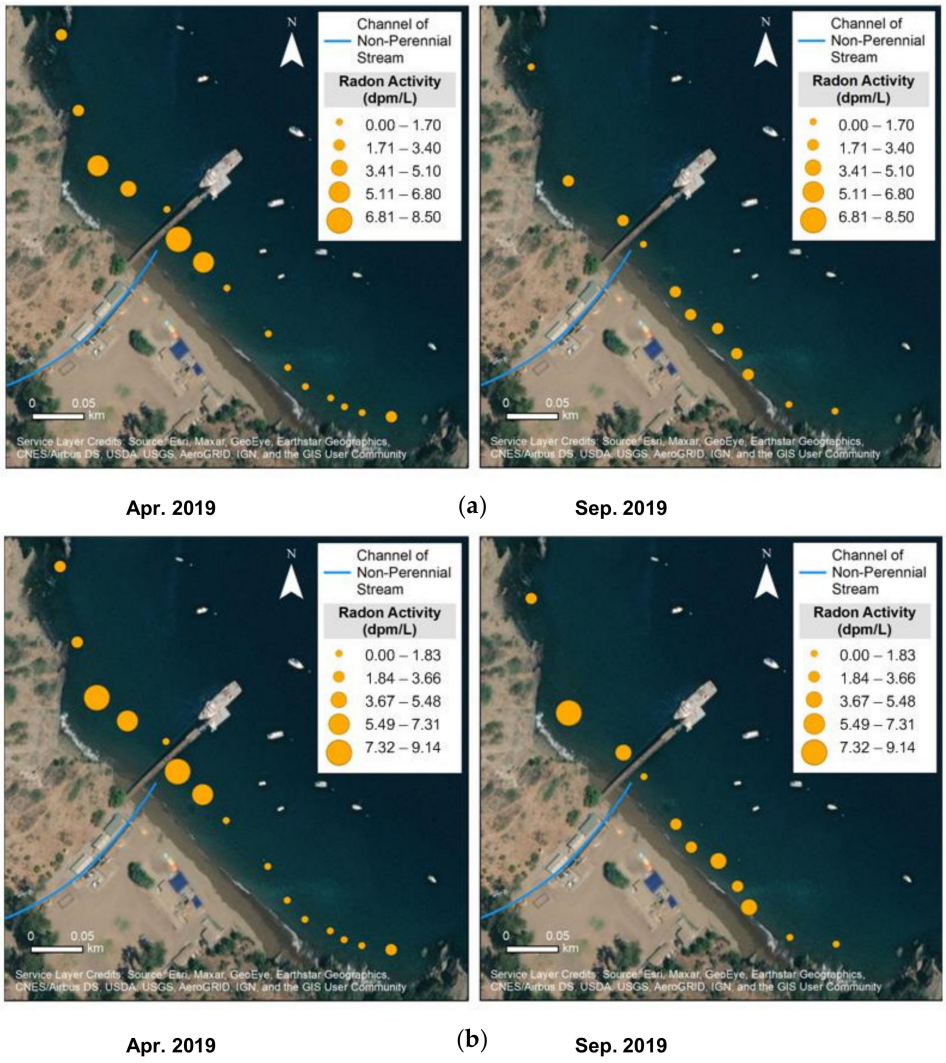

Figure 8. Spatial variation of radon activity in water in Toyon Bay based on April (left) and September (right) 2019 surveys: (**a**) without tidal correction and (**b**) with tidal correction.

The total SGD water fluxes based on the [26] reported saline groundwater radon end-member were estimated at 3.31 $m^3/m/day$ and 5.47 $m^3/m/day$ in April and September 2019, respectively (Table 1). In both April and September 2019, SGD was the largest source of radon, responsible for 94.6% and 96.9%, respectively, of the total radon gains. The largest radon sink was mixing with offshore waters causing 53.4% and 89.4% of the total radon losses in April and September 2019, respectively.

Table 1. Freshwater (f) and recirculated seawater (s) SGD fluxes.

Period	F_{SGDw} ($m^3/m/d$)	f_f	f_s	F_{fSGDw} ($m^3/m/d$)	F_{sSGDw} ($m^3/m/d$)
Apr. 2019	3.31	0.082	0.918	0.27	3.04
Sep. 2019	5.47	0.051	0.949	0.28	5.19
Mean	4.39	0.066	0.934	0.27	4.11

The consistently higher radon values measured in the northern part of Toyon Bay (Figure 8) likely reflect the presence of a shallow alluvial aquifer associated with the non-perennial stream, which was not flowing during either of the sampling campaigns. This permeable aquifer may facilitate enhanced groundwater flow and discharge of diffuse SGD.

Further research on the spatial distribution of these permeable sediments via such methods as electrical resistivity profiling and soil coring [7,51,52] is warranted to test this hypothesis.

SGD in Toyon Bay was identified as mostly saline (Table 1). The FSGD water flux was estimated as 0.27 $m^3/m/day$ in April 2019 and 0.28 $m^3/m/day$ in September 2019, comprising less than 10% of the total SGD water flux in each sampling campaign. The large seawater fraction is again attributed to tidal pumping as salinities showed almost no variation over time and space, hovering between 32.5 and 32.8 ppt in April 2019 and between 33.7 and 33.8 in September 2019. There was also no salinity/radon correlation, which further supports tidal pumping over fresh meteoric water inflow as the controlling SGD mechanism [5,15,48].

The uniform FSGD values determined for both sampling campaigns (~0.27 $m^3/m/day$) are surprising given that some seasonality in response to increased net precipitation and, by implication, steeper hydraulic gradients in the wet season (spring) would be expected. However, the effects of net precipitation may lag as a result of the time required for infiltration and downgradient groundwater flow, so higher-resolution time-series (i.e., groundwater table fluctuation) data are needed to discern this lag, constrain recharge rates [53,54], and capture the bulk FSGD flux from the winter/spring rains in radon and salinity surveys.

3.3. Comparison with Other Studies

The total SGD water fluxes calculated for Toyon Bay were comparable to the values reported in other sites with Mediterranean or semi-arid to arid climate (Table 2). Variation in estimated SGD values reflects differences in hydrogeology, land use/land cover, and study method. For example, a wide range of values reported in La Paz Bay, Mexico, were based on radon data from two distinct sampling locations—one shallow aquifer underlying mangrove wetlands and one deeper aquifer downgradient of rocky headlands and cliffs [5]. The values in Maro-Cerro Gordo and Mallorca Island, Spain, showed large variations due to the use of multiple sampling locations with different lithologies or land uses [1,55]. The variations seen in Donnalucata, Italy, and Marina Lagoon, Egypt, reflect the use of multiple sources for the terrestrial groundwater radon end-members [49,56]. The lower SGD rates seen at Santa Barbara Beach may, despite its geographical proximity to Catalina and similar seasonal coverage, reflect differences in recharge rates, hydraulic gradients, and aquifer composition. Increased wave height (i.e., white caps) at Santa Barbara Beach, which should greatly enhance F_{atm}, could also be important.

Table 2. Total SGD flux comparison.

Climate	Site	Method	Total SGD Flux (m/d)	References
Arid/Semi-Arid	Gulf of Aqaba, Israel	Ra Isotopes	0.06–0.26	Shellenbarger et al. [2]
	Gaza Strip	Radon	0.01–0.06	Mushtaha and Walraevens [4]
	Marina Lagoon, Egypt	Radon	0.02–0.06	El-Gamal et al. [49]
	La Paz Bay, Mexico	Radon	0.02–0.18	Urquidi-Gaume et al. [5]
Mediterranean	False Bay, South Africa	Radon	0.01	Schubert et al. [23]
	Dor Beach, Israel	Radon	0.08	Weinstein et al. [15]
	Donnalucata, Italy	Radon	0.14–0.87	Burnett and Dulaiova [56]
	Mallorca Island, Spain	Seepage Meter	0.004–0.65	Basterretxea et al. [55]
	Maro-Cerro Gordo, Spain	Radon	0.22–0.52	Montiel et al. [1]
	Santa Barbara, CA, USA	Radon	0.03–0.09	Swarzenski and Izbicki [17]
	Toyon Bay, CA, USA	Radon	0.14–0.29	This study

The FSGD water fluxes calculated for Toyon Bay were within the range (i.e., below 0.27 m^2/day) reported for the region in a continental-scale study by Sawyer et al. [57]. In their study, however, no measured geochemical data were used, so direct comparisons should be treated with caution.

The groundwater recharge rates for Catalina Island and the Toyon Bay watershed, based on the SWB model [27], were 0.13 and 0.35 $m^3/m/day$, respectively (Figure 9). In this assessment, SWB estimates of recharge were found to be slightly higher than the estimates from chloride mass balance of groundwater, which may either reflect inaccuracies in the water budget components and/or geochemical processes such as halite dissolution in the unsaturated zone, leading to the potential underestimation of the actual chloride input to groundwater. When compared to our FSGD estimates (mean: 0.27 $m^3/m/day$), the SWB recharge value for Toyon Bay was remarkably similar. As discussed further in our sensitivity analyses, slight differences may be explained by some uncertainty in water depth and the terrestrial groundwater radon end-member used in calculating the SGD water fluxes. While not only the magnitude of the FSGD water fluxes was similar to the SWB study, the spatial variation of radon activities also resembled the pattern of recharge from the SWB model, with highest values towards the north, near the outlet of the non-perennial Toyon stream (compare Figures 8 and 9).

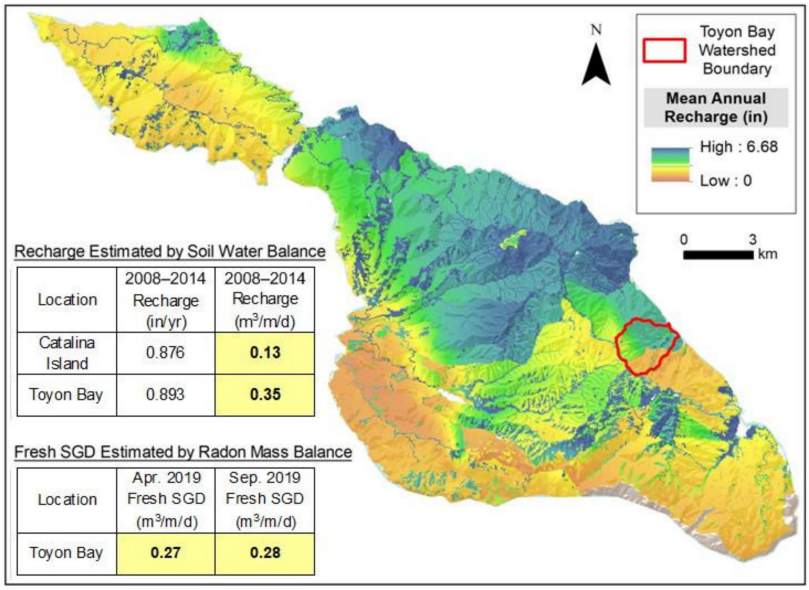

Figure 9. SWB and FSGD modeling-derived estimates of groundwater recharge in Catalina Island and Toyon Bay watershed (modified from [27]).

3.4. Sensitivity Analysis

3.4.1. Effect of Water Depth

Measuring the water depths in SGD surveys can be difficult in some settings due to wave action and uneven seafloor topography. In the sensitivity analysis, using a set of values between 0.50 and 3.00 m for the water depth at the spatial survey sites revealed a positive linear correlation between the water depth and the SGD water flux (Figure 10), reflecting a linear increase in the radon inventory and hence a linear increase in scaling to the time-series data (Equations (2) and (3)). Given this, uncertainty in the water depth of $\pm$0.1 m could very well explain the difference between the FSGD and SWB recharge estimates for Toyon Bay (Figure 9).

3.4.2. Effect of Terrestrial Groundwater Radon End-Member

Defining the terrestrial groundwater radon end-member is one of the major challenges in estimating the SGD flux by radon mass balance because of uncertainty in the sample data from heterogeneous radon distribution in groundwater [23] and lower radon concentrations in tidally recirculated seawater [46]. The measured radon activities from incubation experiments of sand samples of the Cherry Cove, Fourth of July Cove, Isthmus Cove, and Big Fisherman's Cove inlets (Figure 1) were 49,000; 67,000; 91,000; and 267,000 dpm/m^3, respectively. Interestingly, the watershed geology of Big Fisherman's Cove most resembles

that of Toyon Bay (intermediate volcanics and associated sediments), but the incubation experiment-derived radon value was ~2.5 times higher than the value measured at Toyon Spring (~110,000 dpm/m^3). By contrast, the low values measured from the samples of Cherry Cove and Fourth of July Cove align very closely to saline groundwater radon values reported for beach piezometer samples obtained between the high and low tide marks (30,000–50,000 dpm/m^3) [26], which are characterized by significantly shorter residence times than the 30 days in the incubation experiments. For the sensitivity analysis, the SGD water flux was calculated for a set of values between 25,000 and 300,000 dpm/m^3 to bracket the baseline value of 57,000 dpm/m^{3,} as well as those from the incubation experiments and values applied in previous studies at similar settings (Table 3).

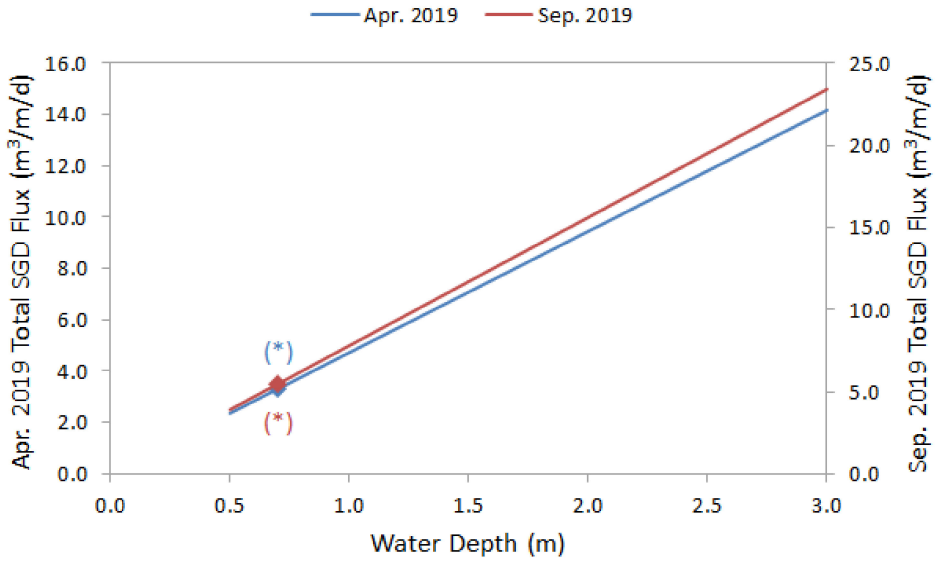

Figure 10. April and September 2019 total SGD water fluxes for different water depths. (*) represents the baseline measured water depth value.

Table 3. Terrestrial groundwater end-member comparison in arid/semi-arid sites.

Site	Terrestrial Groundwater Radon End-Member (dpm/L)	References
Gaza Strip	340–390	Mushtaha and Walraevens [4]
Marina Lagoon, Egypt	113, 298	El-Gamal et al. [49]
La Paz Bay, Mexico	439	Urquidi-Gaume et al. [5]
False Bay, South Africa	288	Schubert et al. [23]
Dor Beach, Israel	242	Weinstein et al. [15]
Donnalucata, Italy	149, 293, 906	Burnett and Dulaiova [56]
Maro-Cerro Gordo, Spain	300, 370	Montiel et al. [1]
Santa Barbara, CA, USA	463	Swarzenski and Izbicki [17]
Toyon Bay, CA, USA	57, (49–267)	Colbert et al. [26], this study

Note: The range for Toyon Bay is based on the values obtained from the incubation experiments and the measured value from the Toyon Spring.

When the terrestrial groundwater end-member radon activity was increased, while other parameters were kept fixed, the SGD flux estimate decreased for both April and September 2019 (Figure 11) because an increase in the terrestrial groundwater end-member radon activity leads to an increase in the diffusive radon input from the seabed sediment and hence a decrease in the SGD radon flux to maintain mass balance. Since the SGD water flux was determined by dividing the SGD radon flux by the terrestrial groundwater end-member radon activity, an increased denominator further lowered the SGD water flux estimate.

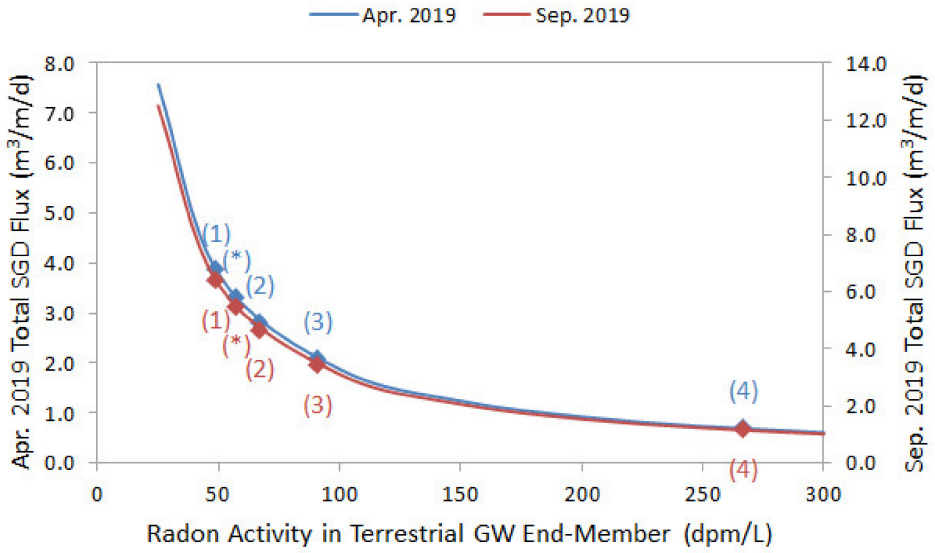

Figure 11. April and September 2019 total SGD water fluxes for different terrestrial groundwater end-members. Lines represent concentration range of 25,000–300,000 dpm/m^3. (*) represents the baseline C_{GW} value. (1) to (4) represent the C_{GW} values estimated by incubation experiments of the Cherry Cove, Fourth of July Cove, Isthmus Cove, and Big Fisherman's Cove beach sand samples, respectively.

Changing the terrestrial groundwater radon end-member exerted the highest relative sensitivity, with a value of 230%, when the terrestrial groundwater radon end-member was at its lowest value. The near-asymptotic trend in the sensitivity of the SGD water flux to the terrestrial groundwater end-member radon activity highlights the importance of an accurate assessment, ideally from concurrently collected surface- and groundwater time-series.

4. Conclusions and Implications

This study highlights the value of radon and salinity mass balance for FSGD and groundwater recharge estimation in a semi-arid coastal watershed. Our main findings are summarized as follows:

- SGD in Toyon Bay was found to be mostly saline with limited freshwater component, where the large seawater component could be associated with tidal pumping. The total SGD fluxes, consisting of both freshwater and seawater components, were generally low in Toyon Bay, and these values were comparable to those reported in other sites with a similar climate.
- The fresh SGD flux was slightly lower than the groundwater recharge rate for the watershed estimated by the SWB model. This finding is consistent with previous results, where the SWB model was found to overestimate recharge compared to the chloride mass balance discerned from groundwater and precipitation data. More work on the temporal patterns of FSGD rates and the chloride mass balance in Toyon Bay groundwater could further refine the recharge estimate and illuminate the effects of recent droughts on recharge magnitude.
- The FSGD fluxes in Toyon Bay were very consistent between April and September 2019, supporting the importance of tidal pumping and mixing with offshore waters on controlling SGD magnitude. Spatial variation in the radon activities in the northern part of Toyon Bay, near a non-perennial stream, suggests underflow through a high-permeability feature below the streambed. Further research is needed to test this hypothesis and ascertain the depth at which the underflow reaches the ocean.
- Sensitivity analyses revealed SGD fluxes to be significantly influenced by uncertainties in the terrestrial groundwater radon end-member and water depth. Using lower values for the former and higher values for the latter would yield higher FSGD rates

closer to the recharge estimates from the SWB model; however, these values may not be within the reasonable ranges for the Toyon Bay setting.

More research on radon dynamics of recirculated seawater is needed for more refined SGD and recharge analysis in similar semi-arid settings. Furthermore, the use of multiple and concurrent radon time-series in nearshore waters is recommended to better assess spatiotemporal patterns of F_{tide} and F_{mix} and account for their influences on FSGD.

Supplementary Materials: The following supporting information can be downloaded at: https://www.mdpi.com/article/10.3390/w14071068/s1, Table S1: April 2019 spatial survey data by site; Table S2. September 2019 spatial survey data by site; Table S3. May 2019 time-series data by hour at site TBTS1; Table S4. September 2019 time-series data by hour at site TBTS2. Results of Figure 3 are presented in Supplementary File S1.

Author Contributions: This work was conceptualized by M.T. and B.H. Both authors contributed equally to the writing and editing of the manuscript. All authors have read and agreed to the published version of the manuscript.

Funding: This research was supported by the Catalina Island Conservancy, NSF grant HS-1936671 and CSU COAST SLR grant 210611.

Acknowledgments: We would like to extend special thanks for fieldwork assistance and manuscript reviews to G. Holk, M. Becker, D. Hammond, L. Dodd, E. Malakoff, S. Levi, J. Malone, M. Ruane, M. Kemp, C. Meadows, J. Lai, M. Enamorado, and M. Nguyen, and the staff of the Catalina Island Marine Institute and the USC Wrigley Marine Science Center.

Conflicts of Interest: The authors declare no conflict of interest.

References

1. Montiel, D.; Dimova, N.; Andreo, B.; Prieto, J.; García-Orellana, J.; Rodellas, V. Assessing Submarine Groundwater Discharge (SGD) and Nitrate Fluxes in Highly Heterogeneous Coastal Karst Aquifers: Challenges and Solutions. *J. Hydrol.* **2018**, *557*, 222–242. [CrossRef]
2. Shellenbarger, G.G.; Monismith, S.G.; Genin, A.; Paytan, A. The Importance of Submarine Groundwater Discharge to the near Shore Nutrient Supply in the Gulf of Aqaba (Israel). *Limnol. Oceanogr.* **2006**, *51*, 1876–1886. [CrossRef]
3. Kim, G.; Lee, K.K. Large Submarine Groundwater Discharge (SGD) from a Volcanic Island. *Geophys. Res. Lett.* **2003**, *30*, 2098. [CrossRef]
4. Mushtaha, A.; Walraevens, K. Quantification of Submarine Groundwater Discharge in the Gaza Strip. *Water* **2018**, *10*, 1818. [CrossRef]
5. Urquidi-Gaume, M.; Santos, I.R.; Lechuga-Deveze, C. Submarine Groundwater Discharge as a Source of Dissolved Nutrients to an Arid Coastal Embayment (La Paz, Mexico). *Environ. Earth Sci.* **2016**, *75*, 154. [CrossRef]
6. Wang, X.; Li, H.; Yang, J.; Zheng, C.; Zhang, Y.; An, A.; Zhang, M.; Xiao, K. Nutrient Inputs through Submarine Groundwater Discharge in an Embayment: A Radon Investigation in Daya Bay, China. *J. Hydrol.* **2017**, *551*, 784–792. [CrossRef]
7. Hagedorn, B.; Becker, M.W.; Silbiger, N.J. Evidence of Freshened Groundwater below a Tropical Fringing Reef. *Hydrogeol. J.* **2020**, *2*, 2501–2517. [CrossRef]
8. Michael, H.A.; Mulligan, A.E.; Harvey, C.F. Seasonal Oscillations in Water Exchange between Aquifers and the Coastal Ocean. *Nature* **2005**, *436*, 1145–1148. [CrossRef]
9. Knee, K.L.; Paytan, A. Submarine Groundwater Discharge. In *Treatise on Estuarine and Coastal Science*; Elsevier: Amsterdam, The Netherlands, 2011; pp. 205–233. ISBN 978-0-08-087885-0.
10. Bishop, J.M.; Glenn, C.R.; Amato, D.W.; Dulai, H. Effect of Land Use and Groundwater Flow Path on Submarine Groundwater Discharge Nutrient Flux. *J. Hydrol. Reg. Stud.* **2017**, *11*, 194–218. [CrossRef]
11. Povinec, P.P.; Burnett, W.C.; Beck, A.; Bokuniewicz, H.; Charette, M.; Gonneea, M.E.; Groening, M.; Ishitobi, T.; Kontar, E.; Liong Wee Kwong, L.; et al. Isotopic, Geophysical and Biogeochemical Investigation of Submarine Groundwater Discharge: IAEA-UNESCO Intercomparison Exercise at Mauritius Island. *J. Environ. Radioact.* **2012**, *104*, 24–45. [CrossRef]
12. Taniguchi, M.; Burnett, W.C.; Dulaiova, H.; Siringan, F.; Foronda, J.; Wattayakorn, G.; Rungsupa, S.; Kontar, E.A.; Ishitobi, T. Groundwater Discharge as an Important Land-Sea Pathway into Manila Bay, Philippines. *J. Coast. Res.* **2008**, *1*, 15–24. [CrossRef]
13. Montiel, D.; Lamore, A.; Stewart, J.; Dimova, N. Is Submarine Groundwater Discharge (SGD) Important for the Historical Fish Kills and Harmful Algal Bloom Events of Mobile Bay? *Estuaries Coasts* **2019**, *42*, 470–493. [CrossRef]
14. Cyronak, T.; Santos, I.R.; Erler, D.V.; Eyre, B.D. Groundwater and Porewater as Major Sources of Alkalinity to a Fringing Coral Reef Lagoon (Muri Lagoon, Cook Islands). *Biogeosciences* **2013**, *10*, 2467–2480. [CrossRef]

15. Weinstein, Y.; Burnett, W.C.; Swarzenski, P.W.; Shalem, Y.; Yechieli, Y.; Herut, B. Role of Aquifer Heterogeneity in Fresh Groundwater Discharge and Seawater Recycling: An Example from the Carmel Coast, Israel. *J. Geophys. Res.* **2007**, *112*, C12016. [CrossRef]
16. Boehm, A.B.; Paytan, A.; Shellenbarger, G.G.; Davis, K.A. Composition and Flux of Groundwater from a California Beach Aquifer: Implications for Nutrient Supply to the Surf Zone. *Cont. Shelf Res.* **2006**, *26*, 269–282. [CrossRef]
17. Swarzenski, P.W.; Izbicki, J.A. Coastal Groundwater Dynamics off Santa Barbara, California: Combining Geochemical Tracers, Electromagnetic Seepmeters, and Electrical Resistivity. *Estuar. Coast. Shelf Sci.* **2009**, *83*, 77–89. [CrossRef]
18. Alfarrah, N.; Walraevens, K. Groundwater Overexploitation and Seawater Intrusion in Coastal Areas of Arid and Semi-Arid Regions. *Water* **2018**, *10*, 143. [CrossRef]
19. Barlow, P.M.; Reichard, E.G. Saltwater Intrusion in Coastal Regions of North America. *Hydrogeol. J.* **2010**, *18*, 247–260. [CrossRef]
20. Werner, A.; Bakker, M.; Post, V.E.A.; Vandenbohede, A.; Lu, C.; Ataie-Ashtiani, B.; Simmons, G.T.; Barry, D.A. Seawater Intrusion Processes, Investigation and Management: Recent Advances and Future Challenges. *Adv. Water Resour.* **2013**, *51*, 3–26. [CrossRef]
21. Burnett, W.C.; Aggarwal, P.K.; Aureli, A.; Bokuniewicz, H.; Cable, J.E.; Charette, M.A.; Kontar, E.; Krupa, S.; Kulkarni, K.M.; Loveless, A.; et al. Quantifying Submarine Groundwater Discharge in the Coastal Zone via Multiple Methods. *Sci. Total Environ.* **2006**, *367*, 498–543. [CrossRef]
22. Burnett, W.C.; Dulaiova, H. Estimating the Dynamics of Groundwater Input into the Coastal Zone via Continuous Radon-222 Measurements. *J. Environ. Radioact.* **2003**, *69*, 21–35. [CrossRef]
23. Schubert, M.; Petermann, E.; Stollberg, R.; Gebel, M.; Scholten, J.; Knöller, K.; Lorz, C.; Glück, F.; Riemann, K.; Weiß, H. Improved Approach for the Investigation of Submarine Groundwater Discharge by Means of Radon Mapping and Radon Mass Balancing. *Water* **2019**, *11*, 749. [CrossRef]
24. Rodellas, V.; Stieglitz, T.C.; Tamborski, J.J.; van Beek, P.; Andrisoa, A.; Cook, P.G. Conceptual Uncertainties in Groundwater and Porewater Fluxes Estimated by Radon and Radium Mass Balances. *Limnol. Oceanogr.* **2021**, *66*, 1237–1255. [CrossRef]
25. Colbert, S.L.; Hammond, D.E.; Berelson, W.M. Radon-222 Budget in Catalina Harbor, California: 1. Water Mixing Rates. *Limnol. Oceanogr.* **2008**, *53*, 651–658. [CrossRef]
26. Colbert, S.L.; Berelson, W.M.; Hammond, D.E. Radon-222 Budget in Catalina Harbor, California: 2. Flow Dynamics and Residence Time in a Tidal Beach. *Limnol. Oceanogr.* **2008**, *53*, 659–665. [CrossRef]
27. Harlow, J.; Hagedorn, B. SWB Modeling of Groundwater Recharge on Catalina Island, California, during a Period of Severe Drought. *Water* **2019**, *11*, 58. [CrossRef]
28. Ballmer, M. *Soil Survey of Santa Catalina Island, California*; U.S. Department of Agriculture, Natural Resources Conservation Service: Washington, DC, USA, 2008; p. 345.
29. Schumann, R.R.; Minor, S.A.; Muhs, D.R.; Groves, L.T.; McGeehin, J.P. Tectonic Influences on the Preservation of Marine Terraces: Old and New Evidence from Santa Catalina Island, California. *Geomorphology* **2012**, *179*, 208–224. [CrossRef]
30. Rowland, S.M. Geology of Santa Catalina Island. *Calif. Geol.* **1984**, *39*, 239–251.
31. PRISM Parameter-Elevation Relationships on Independent Slopes Model—Precipitation Maps. Northwest Alliance for Computational Science and Engineering. 2010. Available online: http://www.prism.oregonstate.edu/ (accessed on 5 November 2019).
32. Mu, Q.; Zhao, M.; Running, S.W. Improvements to a MODIS Global Terrestrial Evapotranspiration Algorithm. *Remote Sens. Environ.* **2011**, *115*, 1781–1800. [CrossRef]
33. Mu, Q.; Heinsch, F.A.; Zhao, M.; Running, S.W. Development of a Global Evapotranspiration Algorithm Based on MODIS and Global Meteorology Data. *Remote Sens. Environ.* **2007**, *111*, 519–536. [CrossRef]
34. Otton, J.K. *The Geology of Radon*; General Interest Publication: Washington, DC, USA, 1992.
35. Swarzenski, P.W. U/Th Series Radionuclides as Coastal Groundwater Tracers. *Chem. Rev.* **2007**, *107*, 663–674. [CrossRef] [PubMed]
36. Petermann, E.; Schubert, M. Quantification of the Response Delay of Mobile Radon-in-Air Detectors Applied for Detecting Short-Term Fluctuations of Radon-in-Water Concentrations. *Eur. Phys. J. Spec. Top.* **2015**, *224*, 697–707. [CrossRef]
37. Corbett, D.R.; Burnett, W.C.; Cable, P.H.; Clark, S.B. A Multiple Approach to the Determination of Radon Fluxes from Sediments. *J. Radioanal. Nucl. Chem.* **1998**, *236*, 247–253. [CrossRef]
38. Luo, M.; Zhang, Y.; Li, H.; Wang, X.; Xiao, K. Submarine Groundwater Discharge in a Coastal Bay: Evidence from Radon Investigations. *Water* **2020**, *12*, 2552. [CrossRef]
39. Oehler, T.; Bakti, H.; Lubis, R.F.; Purwoarminta, A.; Delinom, R.; Moosdorf, N. Nutrient Dynamics in Submarine Groundwater Discharge through a Coral Reef (Western Lombok, Indonesia). *Limnol. Oceanogr.* **2019**, *64*, 2646–2661. [CrossRef]
40. Martens, C.S.; Kipphut, G.W.; Klump, J.V. Sediment-Water Chemical Exchange in the Coastal Zone Traced by in Situ Radon-222 Flux Measurements. *Science* **1980**, *208*, 285–288. [CrossRef] [PubMed]
41. Peng, T.-H.; Takahashi, T.; Broecker, W.S. Surface Radon Measurements in the North Pacific Ocean Station Papa. *J. Geophys. Res.* **1974**, *79*, 1772–1780. [CrossRef]
42. Zappa, C.J.; McGillis, W.R.; Raymond, P.A.; Edson, J.B.; Hintsa, E.J.; Zemmelink, H.J.; Dacey, J.W.H.; Ho, D.T. Environmental Turbulent Mixing Controls on Air-Water Gas Exchange in Marine and Aquatic Systems. *Geophys. Res. Lett.* **2007**, *34*, L10601. [CrossRef]
43. Wanninkhof, R. Relationship between Wind Speed and Gas Exchange over the Ocean Revisited. *Limnol. Oceanogr. Methods* **2014**, *12*, 351–362. [CrossRef]

44. Correa, R.E.; Cardenas, M.B.; Rodolfo, R.S.; Lapus, M.R.; Davis, K.L.; Giles, A.B.; Fullon, J.C.; Hajati, M.-C.; Moosdorf, N.; Sanders, C.J.; et al. Submarine Groundwater Discharge Releases CO2 to a Coral Reef. *ACS EST Water* **2021**, *1*, 1756–1764. [CrossRef]
45. Tait, D.R.; Santos, I.R.; Erler, D.V.; Befus, K.M.; Cardenas, M.B.; Eyre, B.D. Estimating Submarine Groundwater Discharge in a South Pacific Coral Reef Lagoon Using Different Radioisotope and Geophysical Approaches. *Mar. Chem.* **2013**, *156*, 49–60. [CrossRef]
46. Santos, I.R.; Erler, D.; Tait, D.; Eyre, B.D. Breathing of a Coral Cay: Tracing Tidally Driven Seawater Recirculation in Permeable Coral Reef Sediments. *J. Geophys. Res. Oceans* **2010**, *115*, 10. [CrossRef]
47. Elmaghraby, E.K.; Ataalla, N.N.; Afifi, M.B.; Salem, E. Radon Exhalation and Transfer Processes in Aqueous Media. *Eur. Phys. J. Plus* **2021**, *136*, 1217. [CrossRef]
48. Cyronak, T.; Santos, I.R.; Erler, D.V.; Maher, D.T.; Eyre, B.D. Drivers of PCO2 Variability in Two Contrasting Coral Reef Lagoons: The Influence of Submarine Groundwater Discharge. *Glob. Biogeochem. Cycles* **2014**, *28*, 398–414. [CrossRef]
49. El-Gamal, A.A.; Peterson, R.N.; Burnett, W.C. Detecting Freshwater Inputs via Groundwater Discharge to Marina Lagoon, Mediterranean Coast, Egypt. *Estuaries Coasts* **2012**, *35*, 1486–1499. [CrossRef]
50. Wu, Z.; Zhou, H.; Zhang, S.; Liu, Y. Using 222Rn to Estimate Submarine Groundwater Discharge (SGD) and the Associated Nutrient Fluxes into Xiangshan Bay, East China Sea. *Mar. Pollut. Bull.* **2013**, *73*, 183–191. [CrossRef]
51. Befus, K.M.; Cardenas, M.B.; Tait, D.R.; Erler, D.V. Geoelectrical Signals of Geologic and Hydrologic Processes in a Fringing Reef Lagoon Setting. *J. Hydrol.* **2014**, *517*, 508–520. [CrossRef]
52. Dimova, N.T.; Swarzenski, P.W.; Dulaiova, H.; Glenn, C.R. Utilizing Multichannel Electrical Resistivity Methods to Examine the Dynamics of the Fresh Water–Seawater Interface in Two Hawaiian Groundwater Systems. *J. Geophys. Res. C Ocean.* **2012**, *117*, C02012. [CrossRef]
53. Fan, J.; Oestergaard, K.T.; Guyot, A.; Lockington, D.A. Estimating Groundwater Recharge and Evapotranspiration from Water Table Fluctuations under Three Vegetation Covers in a Coastal Sandy Aquifer of Subtropical Australia. *J. Hydrol.* **2014**, *519*, 1120–1129. [CrossRef]
54. Hagedorn, B.; El-Kadi, A.; Mair, A.; Whittier, R.; Ha, K. Estimating Recharge in Fractured Aquifers of a Temperate Humid to Semiarid Volcanic Island (Jeju, Korea) from Water Table Fluctuations, and Cl, CFC-12 and 3H Chemistry. *J. Hydrol.* **2011**, *409*, 650–662. [CrossRef]
55. Basterretxea, G.; Tovar-Sanchez, A.; Beck, A.J.; Masqué, P.; Bokuniewicz, H.J.; Coffey, R.; Duarte, C.M.; Garcia-Orellana, J.; Garcia-Solsona, E.; Martinez-Ribes, L.; et al. Submarine Groundwater Discharge to the Coastal Environment of a Mediterranean Island (Majorca, Spain): Ecosystem and Biogeochemical Significance. *Ecosystems* **2010**, *13*, 629–643. [CrossRef]
56. Burnett, W.C.; Dulaiova, H. Radon as a Tracer of Submarine Groundwater Discharge into a Boat Basin in Donnalucata, Sicily. *Cont. Shelf Res.* **2006**, *26*, 862–873. [CrossRef]
57. Sawyer, A.H.; David, C.H.; Famiglietti, J.S. Continental Patterns of Submarine Groundwater Discharge Reveal Coastal Vulnerabilities. *Science* **2016**, *353*, 705–707. [CrossRef] [PubMed]